Available online at www.sciencedirect.com
SCIENCE DIRECT
International Journal of Heat and Mass Transfer 49 (2006) 2903–2911
International Journal of HEAT and MASS TRANSFER
www.elsevier.com/locate/ijhmt

The effect of a barrier on laminar convection in a box with differentially heated endwalls

Melissa A. Coman *, Graham O. Hughes, Ross C. Kerr, Ross W. Griffiths

Research School of Earth Sciences, The Australian National University, Canberra ACT 0200, Australia

Received 18 April 2005; received in revised form 22 December 2005
Available online 18 April 2006

Abstract

Laminar free convection is studied experimentally in a box with differentially heated endwalls that is divided by a barrier into two connected chambers. We investigate how the steady-state circulation, the temperature field and the transport of heat and mass depend on the height and position of the barrier. We find that the temperature fields in the two chambers are very different and that a complex flow structure develops, featuring a fast overflow of the barrier, a number of shear layers above the barrier, partial boundary layer detrainment on the cold endwall, and a slow upwelling in the cooler of the two chambers. The heat transport is found to have little dependence on the barrier height or barrier position, and begins to decrease rapidly only when the gap above the barrier becomes small.

PACS: 44.25.+f; 47.15.Rq; 47.27.Te; 47.55.Hd

Keywords: Convective exchange; Heat and mass transfer; Laminar convection; Differentially heated cavity; Connected chambers; Barrier

1. Introduction

Laminar convection in a two-dimensional differentially heated box has been extensively studied for a range of aspect ratios, motivated by a wide range of engineering applications [1–10]. At high Rayleigh numbers (about 10^9 in the laminar regime), a strong boundary layer circulation (Fig. 1) accommodates most of the mass and heat fluxes: a buoyant plume rises up the hot endwall, flows along the top of the box, falls down the cold endwall as a dense plume, and then returns along the bottom of the box [3–5]. Fluid in the box interior or 'core' is nearly stagnant and has a temperature field that varies linearly with depth and is independent of longitudinal position [8,10].

However, in many industrial, environmental and geophysical situations convective circulation is strongly influenced by complex building geometries or bottom topographies [11–16]. As a first step towards understanding these more complex flows, this paper explores the effects of placing a barrier on the base of the box that blocks the boundary layer circulation in Fig. 1. We describe how the steady-state convective flow changes as a function of the barrier's height and lateral position, and present measurements of the modified heat and mass transports in the box.

2. Experiments

2.1. Experimental apparatus and procedure

The experiments were carried out in a tank, of length $L = 302$ mm, height $H = 196$ mm and width 150 mm, filled with de-aired water (Fig. 2). The base, lid and sidewalls of the tank were made of Perspex, with heat exchangers as endwalls. Each heat exchanger was kept at a constant temperature by recirculating water from a temperature-controlled bath. The temperature in the heat exchangers was monitored using embedded thermistors. The endwalls had temperatures of 50 °C and 5 °C, giving an applied

* Corresponding author. Tel.: +61 (0)2 6125 9958; fax: +61 (0)2 6257 2737.
E-mail address: melissa.coman@anu.edu.au (M.A. Coman).

0017-9310/$ - see front matter © 2006 Elsevier Ltd. All rights reserved.
doi:10.1016/j.ijheatmasstransfer.2006.02.031

Nomenclature

A	box aspect ratio
c_p	specific heat of water
g	gravitational acceleration
h	barrier height
h_g	size of the opening above the barrier ($=H-h$)
H	tank height
k	thermal conductivity of the fluid
L	tank length
L_1	length of chamber adjacent to the hot endwall
L_2	length of chamber adjacent to the cold endwall ($=L-L_1$)
Nu	Nusselt number
Pr	Prandtl number
Q	heat transport per unit width
Ra	Rayleigh number
R_H	barrier height ratio
R_L	chamber length ratio
u	horizontal flow velocity
V	volume transport per unit width
x	horizontal coordinate (measured from hot endwall)
y	vertical coordinate (measured from base)
Greek symbols	
α	thermal expansion coefficient of the fluid
κ	thermal diffusivity of the fluid
ν	kinematic viscosity of the fluid
ρ	density of water
ΔT	applied temperature difference between the tank endwalls

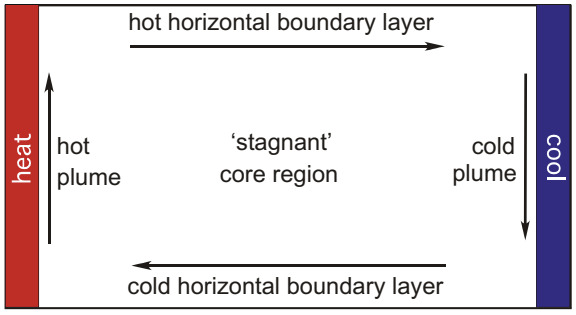

Fig. 1. Schematic of the boundary layer circulation in a differentially heated box at high Rayleigh numbers (no barrier).

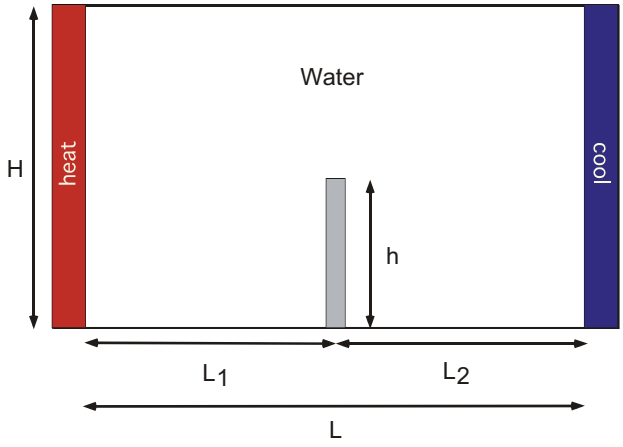

Fig. 2. Experimental configuration (elevation view).

temperature difference ΔT of 45 °C. Holes along the length of the tank in the centre of the lid enabled temperature measurements and flow visualization. This procedure ensured all visualization and measurements were subject to minimal influence from the sidewalls. Barriers, of the same width as the tank and of various heights h, were inserted across the tank at the bottom so as to create two connected chambers with lengths L_1 and $L_2 = L - L_1$. The barriers were made of 20-mm thick Styrofoam to ensure minimal conductive heat transfer through the barrier. Rubber sealing on the three sides of each barrier in contact with the tank prevented water leakage between chambers.

Heat loss from the tank was minimized by double glazed Perspex sidewalls. In addition, the tank was insulated on all sides with 50-mm thick polystyrene foam. The insulation on the two sidewalls was removed only when photographs and temperature profiles were being collected. The heat loss from the tank was found to be minimal, about 1% of the total convective heat flux in the no barrier case.

Two free standing thermistors were placed in the interior of the tank, one in the middle of each chamber. Temperatures were logged as a function of time on a PC and the convective flow was observed to reach thermal equilibrium after about a day. Temperature profiles were measured through the two equilibrated chambers and in the gap above the barrier. The thermistors were accurate to ±0.01 °C and the positions of the thermistors were accurate to ±1 mm. Potassium permanganate crystals and food dye were introduced into the flow through the holes in the tank lid. A slide projector was placed a few metres behind the tank illuminating a sheet of tracing paper attached to the back of the tank. The tracing paper acted as a light diffusing screen, against which the dye could be easily seen. A Nikon D100 digital camera (resolution 1504×1000 pixels) was used to take photos during the experiments. Horizontal velocity measurements were made in the centre of the tank, above the barrier, in order to determine the mass and heat fluxes in the flow. Approximately vertical dye lines were generated by dropping potassium permanganate crystals through the flow. Photographs were taken at intervals between two and sixty seconds, and the velocities

calculated (with an accuracy of ±5%) using the horizontal displacement in dye line positions from one photograph to the next.

2.2. Dimensionless numbers

If we ignore the finite width of the tank (i.e. assume the convective flow is two-dimensional) as well as the non-zero thickness of the barrier, the experimental system is characterized by five dimensionless numbers: the Rayleigh number

$$Ra = \frac{\alpha g \Delta T H^3}{\nu \kappa}, \tag{1}$$

the Prandtl number

$$Pr = \frac{\nu}{\kappa}, \tag{2}$$

the tank aspect ratio

$$A = \frac{H}{L}, \tag{3}$$

the barrier height ratio

$$R_H = \frac{h}{H}, \tag{4}$$

and the chamber length ratio

$$R_L = \frac{L_1}{L}, \tag{5}$$

where α, ν and κ are the thermal expansion coefficient, kinematic viscosity and thermal diffusivity of the fluid and g is the gravitational acceleration.

In this work, R_H was varied by changing the barrier height h, and R_L was varied by changing the lateral position of the barrier (see Table 1). The other parameters were fixed: $Ra = 5 \times 10^9$, $Pr = 7$, and $A = 0.65$. The Grashof number $Gr = Ra/Pr = 0.7 \times 10^9$ was below the value (about 10^9) at which turbulence sets in on a vertical plate [17], so laminar flow was expected in all of our experiments.

Table 1
Dimensionless numbers of the experiments

Experiment	R_H	R_L
1	0	0.5
2	0.18	0.5
3	0.29	0.5
4	0.39	0.5
5	0.49	0.5
6	0.59	0.5
7	0.69	0.5
8	0.80	0.5
9	0.90	0.5
10	0.59	0.25
11	0.59	0.75
12	0.59	0
13	0.59	1.0

3. Experimental results

3.1. Effect of barrier height

To examine the effect of R_H, we conducted nine experiments in which the barrier height was varied, for connected chambers of equal lengths ($R_L = 0.5$; see Table 1). The general flow circulation was similar in all of these experiments. When a barrier was inserted into the tank, water in the cold horizontal boundary layer in Fig. 1 was prevented from flowing all the way to the hot plume. Instead the outflow from the cold plume pooled and slowly filled the right chamber in Fig. 2. Eventually, the coldest water totally filled this chamber to the height of the barrier, creating a 'cold chamber' whose final steady-state temperature profile contrasted dramatically with the temperature profile in the adjacent 'hot chamber' (Fig. 3). The presence of a barrier had a significant effect on the temperature profile at the uppermost levels in the tank only when the gap above the barrier was small (see Fig. 3c).

Figs. 4 and 5 show visualizations of the steady-state convective circulation in experiment 6. A hot laminar plume (not visible) rose up the hot endwall and detrained to form a hot horizontal boundary layer at the top of the tank. Similarly, a cold laminar plume formed at the top of the cold endwall and flowed down the plate, but it split into two at around the height of the barrier. The coldest water from the inner part of the plume (against the endwall) continued to flow downwards, but the water in the outer part of the plume was not cold enough (i.e. dense enough) to penetrate into the cold chamber: it instead detrained and flowed horizontally towards the barrier. Along the way, the intruding flow combined with upwelling water from the cold chamber to produce a strongly stratified overflow at the barrier (see Fig. 7). This flow then plunged over the side of the barrier to form a downflowing plume. Near the base of the barrier the momentum of fluid in the plume caused it to overshoot and oscillate about its level of neutral buoyancy in the heated chamber (Figs. 4 and 5). As the overflow was strongly stratified, only the very coldest water immediately adjacent to the barrier reached the tank bottom, while the remainder entered the interior of the hot chamber at a range of different levels (Fig. 5). This fluid was then gradually drawn towards the lower half of the hot endwall, where it was entrained into the hot plume. In the cold chamber, the flow was primarily driven by the cold sidewall plume, which produced a slow upwelling return flow (cf. [19]). The cold chamber was also affected by stratified withdrawal into the barrier overflow, and by a small amount of heat transfer through the barrier (less than 3% of the total heat transfer) that produced a slow up-flow against the barrier (Fig. 4). Hence a balance between vertical conduction and advection is likely to be involved in maintaining the steady-state vertical temperature gradient in the cold chamber.

The exchange flow above the barrier was found to be strongly dependent on the barrier height (see Fig. 6). In

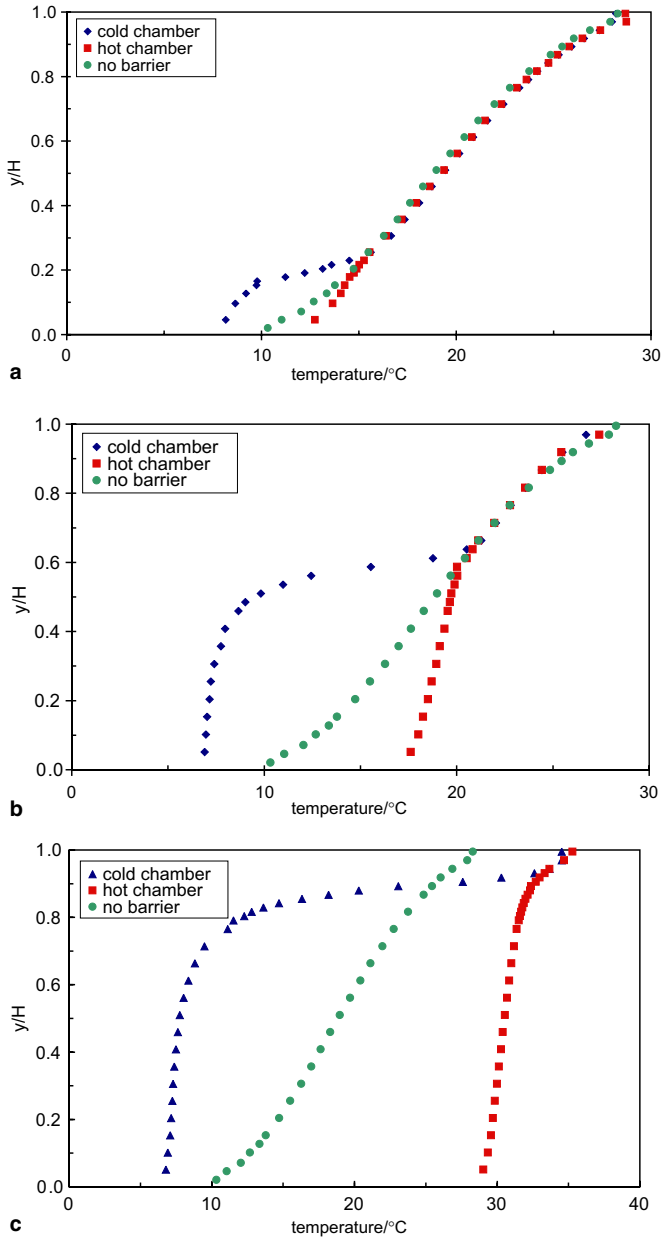

Fig. 3. Steady-state temperature profiles through the two chambers (at $\frac{x}{L} = 0.25$ and 0.75) as a function of barrier height: (a) experiment 2 ($R_H = 0.18$); (b) experiment 6 ($R_H = 0.59$); and (c) experiment 9 ($R_H = 0.9$). The profiles are compared with the steady-state temperature profile at the centre of the tank ($\frac{x}{L} = 0.50$) when no barrier is present (experiment 1).

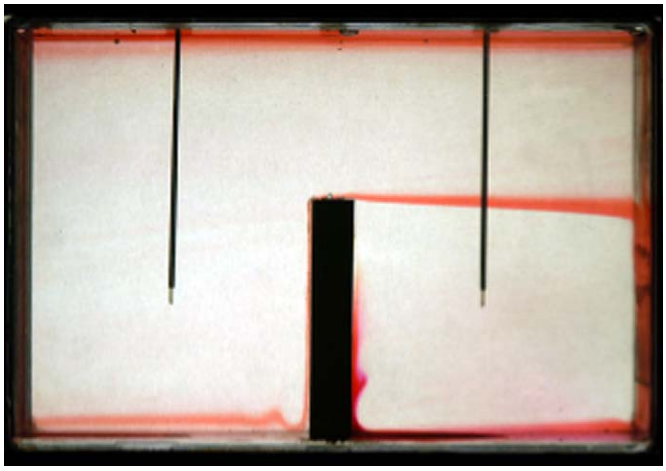

Fig. 4. Visualization of the boundary layer flow for experiment 6. Red dye was introduced into the boundary layer at the bottom of the hot and cold chambers.

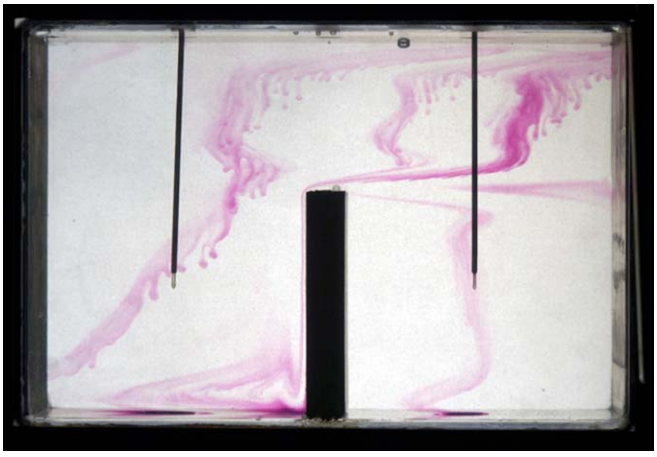

Fig. 5. Visualization of the interior flow for experiment 6. Initially vertical dye streaks were generated by dropping potassium permanganate crystals at three positions: the centre of the tank and aligned horizontally with the thermistors (visible in the centre of each chamber).

the no barrier case (Fig. 6a), we observed strong boundary layer flows at the top and bottom, with a weak uniform shear in the interior (cf. Fig. 1). With the addition of a small barrier (Fig. 6b), the top half of the flow was similar to the no barrier case (Fig. 6a), but the bottom half was significantly different: the return flow occurred in a thinner layer with a much higher velocity. This barrier overflow (like the hot boundary layer reaching the top boundary and the cold boundary layer reaching the base in the case of no barrier) also generated a number of 'shear layers' (cf. [18]), corresponding to local maxima or minima in the horizontal velocity profile. As h was increased, the region of uniform shear in the interior steadily decreased until it disappeared at $R_H = 0.59$ (Fig. 6c). When h was increased further, the number of shear layers decreased from six (for $R_H = 0.59$) to four (for $R_H = 0.69$, see Fig. 6d), and then to a simple bi-directional exchange flow for the highest barrier (Fig. 6e), where a layer of warm water flowed towards the cooled endwall above a cooler layer that overflowed the barrier.

In Fig. 7, the temperature profile above the barrier is shown for a number of different barrier heights. As the barrier height was increased, two main effects were observed. First, the temperature gradient systematically increased in the thin overflow immediately above the barrier, while the gradient above the overflow was almost unchanged. Second, the temperature profiles were shifted to warmer temperatures.

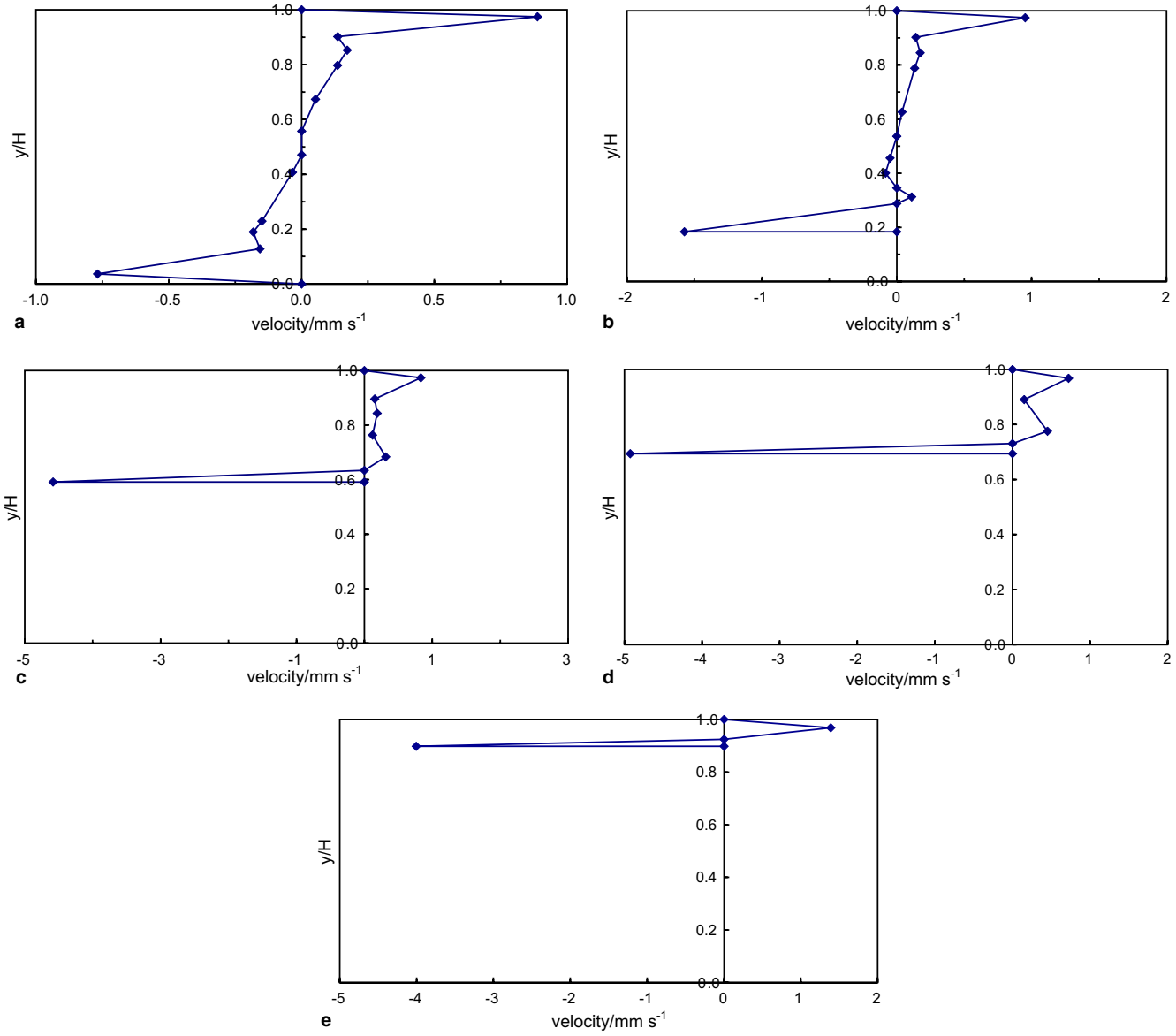

Fig. 6. Velocity profiles above the barrier for (a) $R_H = 0$, (b) $R_H = 0.18$, (c) $R_H = 0.59$, (d) $R_H = 0.69$, (e) $R_H = 0.90$. The points on the plots in (c)–(e) correspond to heights at which the velocity was either zero or a local maximum/minimum. Note that the horizontal scales in (a)–(e) are different.

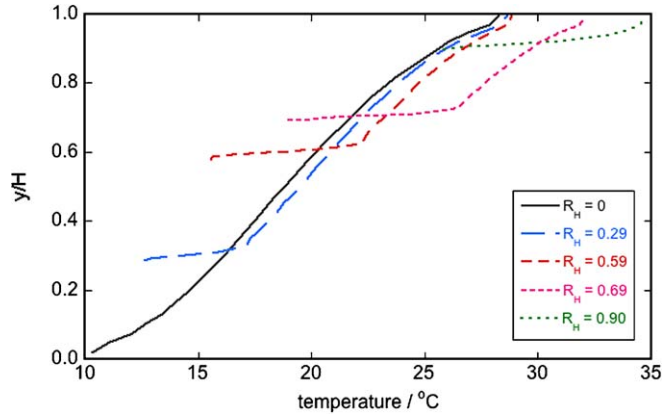

Fig. 7. Temperature profiles above the barrier for $R_H = 0, 0.29, 0.59, 0.69, 0.90$.

From integration of the velocity profiles in Fig. 6, we determined the volume transport per unit width V from the hot chamber to the cold chamber, as a function of the barrier height (Fig. 8). The volume transport had an accuracy of $\pm 10\%$. For modest barrier heights, the transport was found to be relatively constant (and there is a suggestion of a maximum at around $R_H \sim 0.4$). However, when the barrier height became very large ($R_H > 0.8$), the transport decreased rapidly (which satisfies the constraint that the volume transport must go to zero as $h \to H$ and the gap closes).

From the measured velocity and temperature profiles, we determined the heat transport per unit width Q above the barrier

$$Q = \rho c_p \int_h^H uT \, \mathrm{d}y, \tag{6}$$

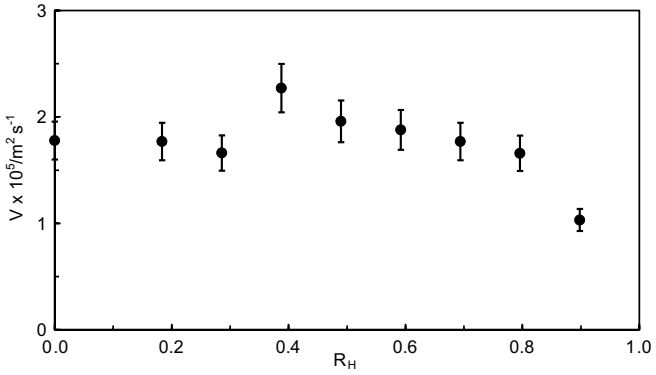

Fig. 8. Volume transport per unit width exchanged through the gap above the barrier as a function of R_H.

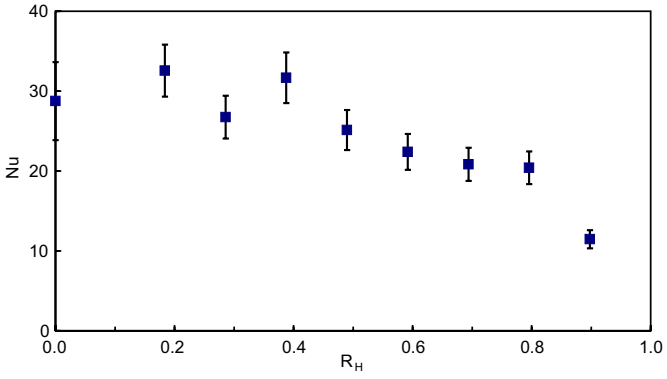

Fig. 9. Nusselt number as a function of R_H.

where ρ is the water density, y is the vertical coordinate and c_p is the specific heat of water at constant temperature. The heat transport had an accuracy of $\pm 10\%$, which was almost entirely due to the uncertainty in the velocity profile. (We note that we have neglected the horizontal conductive heat flux in Eq. (6), which is $\approx 2\%$ of the advected heat flux in these high Rayleigh number experiments, and is negligible compared to the measurement error in Q.) A Nusselt number can then be defined as

$$Nu = \frac{Q}{k\Delta T}, \tag{7}$$

where k is the thermal conductivity of water. The measured Nusselt number is plotted in Fig. 9 as a function of barrier height ratio R_H. No decrease in the heat transport was observed for modest barrier heights, and a rapid decrease in heat transport was found only when $R_H > 0.8$ (satisfying the constraint that the heat transport must go to zero as $h \to H$).

3.2. Effect of barrier position

To examine the effect of R_L, experiment 6 was combined with four further experiments (see Table 1) in which the barrier position was varied but the barrier height was held constant ($R_H = 0.59$). In experiments 10 and 11, the barrier was placed one-quarter and three-quarters of the tank length from the heated endwall, respectively, while in experiments 12 and 13, the barrier was placed against the hot and cold endwall, respectively.

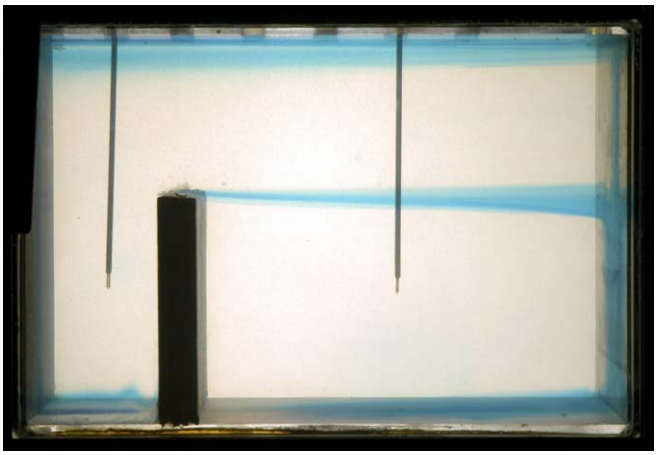

Fig. 10. Visualization of the boundary layer flow for experiment 10. Blue dye was introduced into the boundary layer at the bottom of the hot chamber.

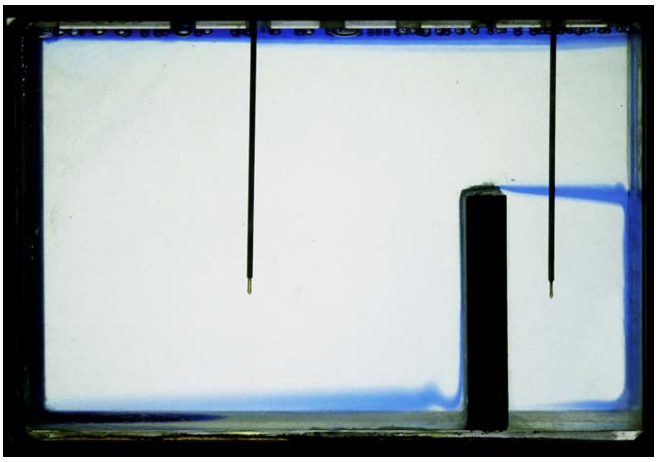

Fig. 11. Visualization of the boundary layer flow for experiment 11. Blue dye was introduced into the boundary layer at the bottom of the hot chamber.

The boundary layer circulation for experiments 10 and 11 (see Figs. 10 and 11) was found to be qualitatively the same as in experiment 6 (Fig. 4). In particular, the position of the barrier did not affect the ponding of cold dense fluid to form a 'cold chamber'. In each case, the cold plume split at the height of the barrier, into an inner plume that continued down the wall to the bottom of the tank and an outer part of the plume that detrained and then flowed horizontally towards the barrier. There was little change in the convective flow in the 'hot chamber', which was still dominated by the cold plume overflowing the barrier and the hot laminar plume rising up the hot endwall.

The similarity of the convective flows in experiments 6, 10 and 11 is seen in both temperature profiles in the 2 chambers (Fig. 12) and velocity profiles above the barrier (Fig. 13). In experiment 13, placing the barrier against the cold endwall eliminated the 'cold chamber', but had little effect on either the temperature profile (Fig. 12) or the velocity profile (compare Fig. 14b with Fig. 6a) measured in the 'hot chamber'. The observed minimal dependence on barrier position is due to the ponding of cold dense fluid below the height of the barrier, which limits the interaction of the convective flow with the cold endwall, wherever the barrier is positioned.

In experiment 12, placing the barrier against the hot endwall limits the interaction of the convective flow with the hot endwall and prevents any barrier overflow. This results in a significant change in both the temperature profile (Fig. 12) and velocity profile (compare Fig. 14a with Figs. 5 and 13) measured in the 'cold chamber', especially above the height of the barrier.

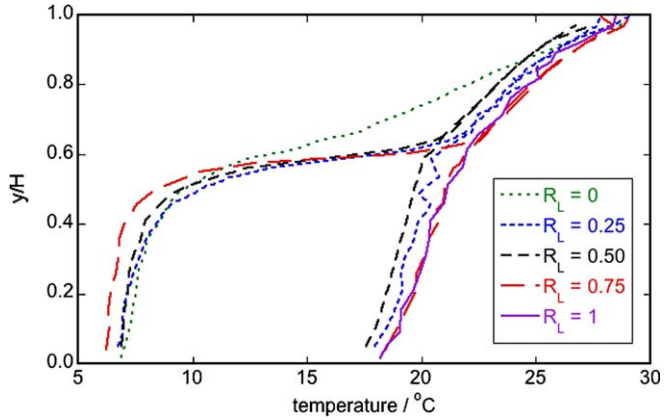

Fig. 12. Steady-state temperature profiles through the two chambers for experiments 6 (at $\frac{x}{L} = 0.25$ and 0.75) , 10 (at $\frac{x}{L} = 0.125$ and 0.625) and 11 (at $\frac{x}{L} = 0.375$ and 0.875), and through the single chamber (at $\frac{x}{L} = 0.50$) in experiments 12 and 13.

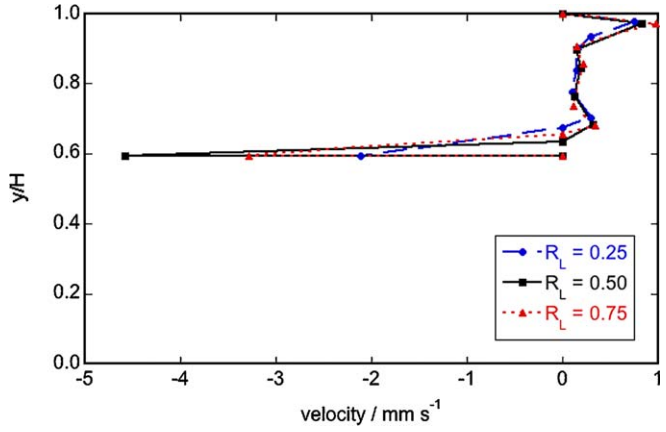

Fig. 13. The velocity profiles above the barrier ($\frac{x}{L} = 0.50$) for different values of R_L (experiments 6, 10 and 11).

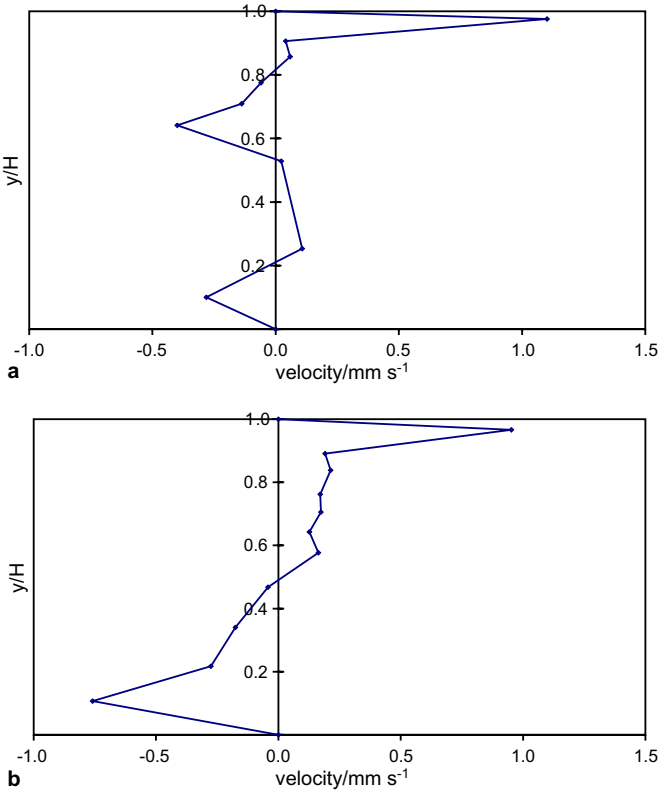

Fig. 14. The velocity profiles through the single chamber in (a) experiment 12 ($R_L = 0$) and (b) experiment 13 ($R_L = 1$).

From the measured velocity and temperature profiles, we also determined both the volume and heat transport per unit width from the hot chamber to the cold chamber, as a function of the barrier position. We found that moving the barrier towards the cold endwall results in a systematic increase in the volume transport (Fig. 15), but has little effect on the heat transport (Fig. 16).

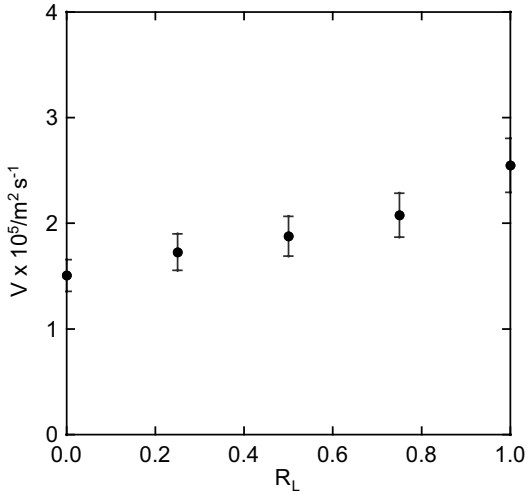

Fig. 15. Volume transport V (●) per unit width as a function of R_L, for $R_H = 0.59$.

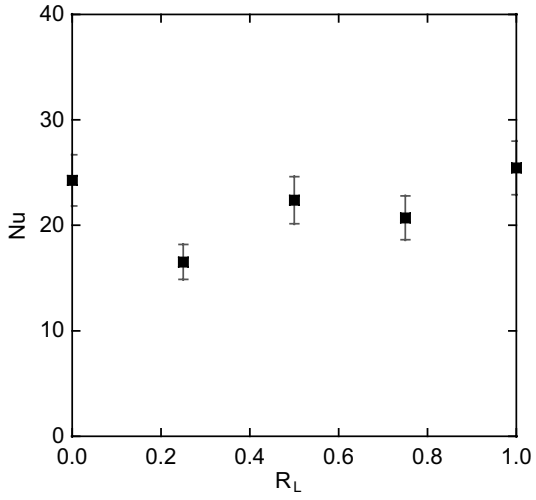

Fig. 16. Nusselt number (■) as a function of R_L, for $R_H = 0.59$.

4. Discussion of heat transfer results

In our experiments, the major impact of the barrier was the creation of the 'cold chamber'. The small temperature difference between the fluid in this cold chamber and the cold endwall implies that most of the heat transfer from this endwall must occur above the height of the barrier. It is therefore interesting to compare our results with a simple model where we assume that the heat transfer is effectively controlled by the gap height $h_g = H - h$. In a rectangular cavity with height h_g, length L, and aspect ratio h_g/L (assumed small), the heat transfer in the boundary layer regime is independent of aspect ratio and given by $Nu(h_g) \propto (\alpha g \Delta T h_g^3/\nu\kappa)^{\frac{1}{5}}$ [5,6]. In Fig. 17, our heat transfer results are therefore replotted in the form $Nu(h_g)/Nu(H)$ as a function of h_g/H, where they are compared with the simple model prediction of $Nu(h_g)/Nu(H) = (h_g/H)^{3/5}$. We find that the model gives a good qualitative guide and understanding of the effect of the barrier. However, the model somewhat underestimates the observed dependence on gap height, which is not surprising as it takes no account of additional heat transfer through the endwalls below the barrier height.

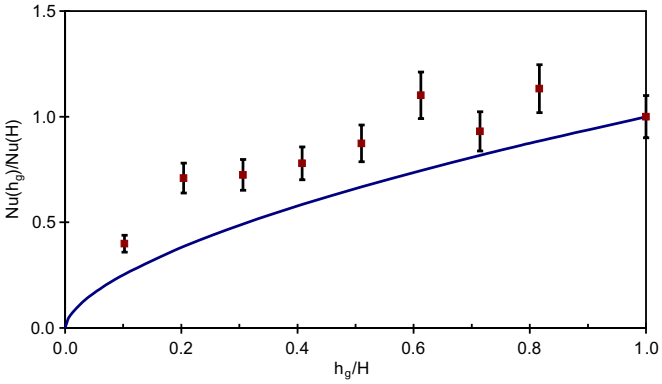

Fig. 17. $Nu(h_g)/Nu(H)$ as a function of $h_g/H = 1 - R_H$ for $R_L = 0.5$.

5. Conclusions

We have studied the convective flow in two connected chambers by placing a partial-height barrier across the base of a box with differentially heated endwalls. The introduction of the barrier severely disrupts the transport of heat and mass in the boundary layers adjacent to the box endwalls and base. Temperature profiles in the box are dramatically modified, with the formation of a very cold chamber and a moderately warmer chamber. A complex flow structure arises, featuring a fast overflow of the barrier, a varying number of shear layers above the barrier, partial boundary layer detrainment on the cold endwall, and slow upwelling in the cold chamber. Interestingly, the heat (and mass) transport is little changed by small and medium-sized barriers, and only begins to decrease rapidly when the barrier height becomes very large (in excess of 80% of the box height). The heat transport is also little changed by the lateral position of the barrier.

We expect that the results in this paper will be useful in predicting the effect of a barrier on laminar convection at high Rayleigh numbers in some industrial and environmental situations. In other situations, such as most geophysical flows, the Rayleigh numbers are likely to be large enough that the overflow and boundary layer flows will all be turbulent (cf. [15]), which might lead to very different behaviour. We look forward to studying this convective flow regime in the future. Further work will also examine the differing advective and conductive timescales that characterize the adjustment to equilibrium in this flow.

Acknowledgements

Technical assistance from Tony Beasley and Brad Ferguson is gratefully acknowledged.

References

[1] A.E. Gill, The boundary layer regime for convection in a rectangular cavity, J. Fluid Mech. 26 (1966) 515–536.
[2] D.E. Cormack, L.G. Leal, J. Imberger, Natural convection in a shallow cavity with differentially heated end walls. Part 1. Asymptotic theory, J. Fluid Mech. 65 (1974) 209–229.
[3] D.E. Cormack, L.G. Leal, J.H. Seinfeld, Natural convection in a shallow cavity with differentially heated end walls. Part 2. Numerical solutions, J. Fluid Mech. 65 (1974) 231–246.
[4] J. Imberger, Natural convection in a shallow cavity with differentially heated end walls. Part 3. Experimental results, J. Fluid Mech. 65 (1974) 247–260.
[5] A. Bejan, C.L. Tien, Laminar natural convection heat transfer in a horizontal cavity with different end temperatures, J. Heat Transfer 100 (1978) 641–647.
[6] A. Bejan, A synthesis of analytical results for natural convection heat transfer across rectangular enclosures, Int. J. Heat Mass Transfer 23 (1980) 723–726.
[7] J. Patterson, J. Imberger, Unsteady natural convection in a rectangular cavity, J. Fluid Mech. 100 (1980) 65–86.
[8] A. Bejan, A.A. Al-Homoud, J. Imberger, Experimental study of high-Rayleigh number convection in a horizontal cavity with different end temperatures, J. Fluid Mech. 109 (1981) 283–299.

[9] P.G. Simpkins, T.D. Dudderar, Convection in rectangular cavities with differentially heated end walls, J. Fluid Mech. 110 (1981) 433–456.
[10] P.G. Simpkins, K.S. Chen, Convection in horizontal cavities, J. Fluid Mech. 166 (1986) 21–39.
[11] O.M. Phillips, On turbulent convection currents and the circulation of the Red Sea, Deep-Sea Res. 13 (1966) 1149–1160.
[12] T. Maxworthy, Convection into domains with open boundaries, Annu. Rev. Fluid Mech. 29 (1997) 327–371.
[13] P.F. Linden, The fluid mechanics of natural ventilation, Annu. Rev. Fluid Mech. 31 (1999) 201–238.
[14] T.D. Finnigan, G.N. Ivey, Convectively driven exchange flow in a stratified sill-enclosed basin, J. Fluid Mech. 418 (2000) 313–338.
[15] A.B.D. Wong, R.W. Griffiths, Two-basin filling boxes, J. Geophys. Res. 106 (2001) 26929–26941.
[16] Y.J.P. Lin, P.F. Linden, Buoyancy-driven ventilation between two chambers, J. Fluid Mech. 463 (2002) 293–312.
[17] J.S. Turner, Buoyancy Effects in Fluids, Cambridge University Press, UK, 1979.
[18] A.B.D. Wong, R.W. Griffiths, G.O. Hughes, Shear layers driven by turbulent plumes, J. Fluid Mech. 434 (2001) 209–241.
[19] M.G. Worster, A.M. Leitch, Laminar free convection in confined regions, J. Fluid Mech. 156 (1985) 301–319.